

Study of coupled-cluster correlations on electromagnetic transitions and hyperfine structure constants of W VI

Anal Bhowmik,¹ Narendra Nath Dutta,² Sourav Roy,³ and Sonjoy Majumder^{1,*}

¹*Department of Physics, Indian Institute of Technology Kharagpur, Kharagpur-721302, India.*

²*Department of Chemistry and Biochemistry, Auburn University, Alabama-36849, USA.*

³*Department of Chemistry, Ben-Gurion University of the Negev, Beer-sheva-84105, Israel.*

Abstract

This work presents precise calculations of important electromagnetic transition amplitudes along with detail of their many-body correlations using relativistic coupled cluster method. Studies of hyperfine interaction constants, useful for plasma diagnostic, with this correlation exhaustive many-body approach are another important area of this work. The calculated oscillator strengths of allowed transitions, amplitudes of forbidden transitions and lifetimes are compared with the other theoretical results wherever available and they show a good agreement. Hyperfine constants of different isotopes of W VI, presented in this paper will be helpful to get accurate picture of abundances of this element in different astronomical bodies.

* sonjoym@phy.iitkgp.ernet.in

I. INTRODUCTION

Recent EBIT experiment [1] on extreme ultraviolet emission for few-times ionized tungsten motivates further study of the forbidden transitions in optical and near-infrared region as plasma diagnostic. The use of tungsten as plasma facing materials attracts the interests of the scientists involved in tokamaks [2–4]. Though tungsten is available in nature as metal with body-center cubic structure, the presence of W^{5+} in particular glasses [5] dictates the behavior of the glasses in magnetic field through the electron paramagnetic resonance (EPR) of the ion. Therefore, precise values of magnetic dipole transitions becomes important here. Recent work [6] shows the important of the study of hyperfine structure constant of this ion for the EPR estimation using crystal field theory. There have been many scientific studies on material containing neutral or ionized tungsten where detail spectroscopic data of these ions are required [7–9]. These spectroscopic data are mainly aimed towards ionization energies of low-lying fine structure, hyperfine levels, and various transition mechanisms among them.

Recent works of Safranova et al. [10] showed long lived highly ionized atoms can be a excellent candidate for the frequency standard or to study α variation. And the system, considered here, is ideal for infrared ion clock whose hyperfine levels requires to estimate precisely. The first excited state of this ion, $5d_{5/2}$, is a metastable state with the ground state, $5d_{3/2}$. Therefore, the lifetime of this metastable state is important in order to use it as a fusion device in plasma medium [11]. All the forbidden lines among the low lying states of this ion are sensitive to the collisional de-excitations and present as indicators of electron density and temperature in the emission region in the study of astrophysics [12, 13] and laboratory tokamak plasmas [14]. To have precise excitation energy in plasma atmosphere, the estimations of hyperfine splittings, in other word hyperfine structure constants, of the system are indispensable. Due to the extremely high lifetimes of the few isotopes of this element, the spectroscopic study of tungsten and its highly stripped ions may take important role in the prediction of age and the procedure of formation and evolution of the astronomical bodies [15, 16]. Moreover, the technological developments of the high-resolution spectrometers increase the demand of the study of hyperfine structures of the various isotopes of this ion for different astrophysical purposes [17–19].

The excitation energies [20–27], oscillator strengths [28], radiative rates [23–25, 29], autoionization rates [23–25] , dielectronic satellite lines [23–25, 28], and dielectronic recom-

bination rates [23–25, 28–40] of various tungsten ions have been studied in several recent literatures both theoretically and experimentally. Safronova *et al.* [28] calculated some of the oscillator strengths of electric dipole transitions of W VI using the relativistic all-order many-body perturbation theory with single and double excitations (SD). Yoca *et al.* [41] and Migdalek *et al.* [42] calculated the oscillator strengths of a number of transitions of this ion using core polarization augmented relativistic Hartree-Fock method, which they named as HFR+CPOL and DF+CP, respectively. All these results motivate us to reinvestigate those transitions. Many-body correlations study is very important here as $3d$, $4d$ and $4f$ are core orbitals. Form our earlier papers [43, 44], it is expected that we will get significant effect of pair correlation for these forbidden transitions. Therefore, the discrepancies between the results demand to have correlation exhaustive relativistic *ab initio* calculations for allowed and forbidden transitions of W VI. Here we apply highly correlated coupled-cluster theory [44, 45] on a relativistic platform (RCC) to calculate the various line parameters of allowed and forbidden transitions as well as the hyperfine structure constants of few low-lying energy levels for this ion.

II. THEORY

A brief introduction of the formalism of our calculation using the coupled-cluster theory is discussed here and details of the mechanism available in our old earlier publications [43, 45]. The coupled-cluster theory is one of the well-known many-body methods [46–53] that allows one to write the atomic or ionic wavefunction for a single valence system using the expression:

$$|\Psi_v\rangle = e^T \{1 + S_v\} |\Phi_v\rangle. \quad (1)$$

Here we assume that the valence electron occupies the ' v 'th orbital of the atom or ion. $|\Phi_v\rangle = a_v^\dagger |\Phi_0\rangle$, where $|\Phi_v\rangle$ and $|\Phi_0\rangle$ are the DF wavefunctions for single valence open shell and closed shell systems, respectively. The operators T and S_v produce single to multiple electron excitations with respect to the reference $|\Phi_0\rangle$ and $|\Phi_v\rangle$, respectively. However, in this present case, we consider these excitations up to the level of single and double only. Some valence triple excitations are also included in the present formalism using a perturbative treatment [43]. Such approximation of the coupled-cluster theory to generate highly correlated wavefunctions is well-known as coupled-cluster with single, double and

valence triple excitations (CCSD(T)) method and is well established as indicated in our earlier works [44, 54–59].

The general matrix element of any arbitrary operator \hat{O} can be expressed in the framework of the RCC theory as,

$$\begin{aligned} O_{k \rightarrow i} &= \frac{\langle \Psi_k | \hat{O} | \Psi_i \rangle}{\sqrt{\langle \Psi_k | \Psi_k \rangle \langle \Psi_i | \Psi_i \rangle}} = \frac{\langle \Phi_k | \{1 + S_k^\dagger\} e^{T^\dagger} \hat{O} e^T \{1 + S_i\} | \Phi_i \rangle}{\sqrt{\langle \Phi_k | \{1 + S_k^\dagger\} e^{T^\dagger} e^T \{1 + S_k\} | \Phi_k \rangle \langle \Phi_i | \{1 + S_i^\dagger\} e^{T^\dagger} e^T \{1 + S_i\} | \Phi_i \rangle}} \\ &= \frac{1}{N} [\bar{O} + (\bar{O} S_{1i} + cc) + (\bar{O} S_{2i} + cc) + \dots] \end{aligned} \quad (2)$$

Here, N is the normalization factor. The single-electron reduced matrix elements corresponding to the electric dipole ($E1$), electric quadrupole ($E2$), and magnetic dipole ($M1$) transition operators are discussed in detail in many references. [55, 60, 61].

In the last equality of the expression 2, the difference of matrix element $\bar{O} = e^{T^\dagger} O e^T$ from O yields the contribution of core correlation. The lowest order Bruckner pair-correlation effect in these matrix elements is considered by the term $\bar{O} S_{1i} + cc$, where cc stands for complex conjugate. The core polarization effect is calculated from the term $\bar{O} S_{2i} + cc$. However, in addition to these, there are other higher-order coupled-cluster terms, like, $S_k^\dagger \bar{O} S_i + cc$ and normalization correction to a wavefunction which are included in the present theoretical approach. A detail explanation of the different correlation contributing factors is available in one of our recent paper [45].

The expression of the oscillator strength and transition probabilities (in s^{-1}) for allowed and forbidden transitions are well known [54, 58, 62]. The lifetime τ_k of a state k can be calculated by considering all different channels of emissions to the states i from k ,

$$\tau_k = \frac{1}{\sum_i A_{k \rightarrow i}}, \quad (3)$$

where $A_{k \rightarrow i}$ represents the probability of the transition from k to i .

The hyperfine energy shift of an atom or ion is given by [59, 63, 64]

$$H_{\text{hfs}} \approx \frac{AK}{2} + \frac{1}{2} \frac{3K(K+1) - 4J(J+1)I(I+1)}{2I(2I-1)2J(2J-1)} B. \quad (4)$$

Here $K = F(F+1) - I(I+1) - J(J+1)$. A and B are the two well-known hyperfine structure constants [64]. The constant A is associated with the magnetic dipole moment of the nucleus. The constant B corresponds to the electric quadrupole moment of the nucleus. The mathematical expressions to calculate these constants for single valence systems

(considering v -th orbital is the valence orbital with relativistic quantum number κ_v) are as follows [61]:

$$\begin{aligned} A &= \mu_N g_I \frac{\langle J || \mathbf{T}^{(1)} || J \rangle}{\sqrt{J(J+1)(2J+1)}} \\ &= -\frac{g_I \kappa_v}{j_v(j_v+1)} \langle v | \frac{1}{r^2} | v \rangle \times 13074.7 \text{MHz} \end{aligned} \quad (5)$$

and

$$\begin{aligned} B &= 2eQ \sqrt{\frac{2J(2J-1)}{(2J+1)(2J+2)(2J+3)}} \langle J || \mathbf{T}^{(2)} || J \rangle, \\ &= Q \frac{2j_v - 1}{2j_v + 2} \langle v | \frac{1}{r^3} | v \rangle \times 234.965 \text{MHz} \end{aligned} \quad (6)$$

where μ_N is the nuclear magneton, g_I is the nuclear g -factor and Q is the quadrupole moment of the nucleus. $\mathbf{T}^{(1)}$ and $\mathbf{T}^{(2)}$ are the two operators which depend on the inverse radial powers of all the electronic coordinates. Their single-particle reduced matrix element forms are discussed explicitly in literature[64].

III. RESULTS AND DISCUSSIONS

For our calculations of different transitions and hyperfine properties, we consider Fermi type of nuclear charge distribution function. The basis-set expansion technique [65] is used here to construct the single-particle DF orbitals as discussed in Eq. 1, where each radial basis function is considered to have the Gaussian-type form. The radial dependence of these Gaussian functions are determined by optimizing two radial parameters α_0 and β [65]. In order to find these optimized parameters, we compare the results of expectation values of $\langle r \rangle$, $\langle 1/r \rangle$, and energies of the DF orbitals among the above basis set expansion method and sophisticated numerical approach, the GRASP92 program [66]. This comparison leads to an extremely good agreement between the corresponding expectation values at $\alpha_0 = 0.00525$ and $\beta = 2.70$. The number of Gaussian functions considered to generate the DF orbitals of s , p , d , f , g and h symmetries are 33, 30, 28, 25, 21 and 20, respectively. However, due to the computational limit, the number of active DF orbitals for the RCC calculations are restricted to 16, 15, 15, 14, 11, and 7, respectively, from the lowest energies of the above mentioned symmetries. Here the selection criteria of number of active DF orbitals employed in the RCC calculations decided by the convergence of core correlation energy at the closed

shell system. In the following discussions, wherever the correlation contribution (δ_{corr}) is mentioned, it indicates the difference between the RCC and the DF results.

Fig. 1 shows the Coulomb-correlation contributions to the ionization potentials with respect to the DF results along with its relativistic effect (Gaunt interaction). One can see from the figure that $5f_{5/2,7/2}$ states are maximally correlated (around 3.5%). All the other states have correlation contributions within 1.0% to 2.3%. Gaunt contributions to the ionization potential are too small, compared to correlation contributions. It varies from -0.04% to 0.06% as shown in the figure.

Electric dipole ($E1$) transition amplitudes calculated at the DF and the RCC levels are presented in Table I along with the different correlation contributions. The wavelengths are estimated from the excitation energies given by the NIST website [67] wherever available, otherwise by using the RCC ionization potentials. The results are calculated using both the length and velocity gauge forms, and are found good agreement within 8% in average. It is known that the velocity gauge values are less stable compared to length gauge values [68], and therefore, the latter gauge values are used commonly for the calculations of astrophysically important parameters, like, oscillator strengths, transition rates and lifetime. The length gauge values for all the transitions are correlated at the level of 10% or more than that, except the transitions associated with the $7s_{1/2}$ and $8s_{1/2}$ states. Important correlation, like, core correlation (Core corr), core polarization (Core pol) and pair correlation (Pair corr) contributions to the total correlation in the different $E1$ transition amplitudes are also highlighted in the table. The difference between δ_{corr} and the sum of the correlations from these three terms provides the correlation contributions from the higher-order terms and normalization corrections to the wave functions as discussed in the theory section. Though our results support the conclusion of Yoca *et al.* [41] that the core polarization contributions are the most important among the other correlation effects here, the pair correlation contributions are significant and in some cases, like, $5f_{5/2,7/2} \rightarrow 5g_{7/2,9/2}$ transitions, are comparable. To understand the source of strong contributions of the core polarization its direct and exchange contributions [69] (representing topologically distinct core polarization diagrams) are studied in Fig. 2. Physically, these diagrams contain electromagnetic interactions between the valence and one of the core electrons to excite two intermediate orbitals and de-excite back to original orbital states. Therefore, they give the leading correlation contributions. Its clear from the figure that the opposite sign among the direct and exchange

parts is significant for the large contributions of the total core polarization. Distinct features observed for $6s_{1/2} \rightarrow 7p_{1/2,3/2}$ where strong correlation contributions observed, as also seen by Migdalek and Siegel [42].

In Table II, our calculated weighted oscillator strengths of the $E1$ transitions are presented in the length and velocity gauges forms and compared with the corresponding SD results [28], HFR+CPOL [41] and DF+CP [42]. They all are falling in the vacuum ultra-violet (UV) region of the electromagnetic spectrum except the transitions $7s_{1/2} \rightarrow 7p_{1/2,3/2}$, which are in middle UV and near UV region. We calculate these oscillator strength values using our calculated matrix elements and experimental wavelengths, wherever available and so as the approaches by others whose calculations are available based on length gauge only. Therefore, differences among the oscillator strengths obtained from the various methods must come from the corresponding $E1$ amplitudes. Table shows that good agreement in the results among different gauges in most of the transitions.

The $E2$ transition amplitudes with different correlation contributing terms are tabulated in Table III along with the corresponding transition wavelengths. They are either falling in the UV or infra-red (IR) regions apart from $6p_{1/2} \rightarrow 6p_{3/2}$, which emits yellow light. There are a few transitions available in literature using the HFR+CPOL method [41] and are good agreement with our results. Unlike, $E1$ transitions, here pair correlation is very strong in many transitions and in some cases, like, transition from the $5f_{5/2,7/2}$ are the lion share in correlation. The strong $E2$ transition amplitudes are estimated for $5f_{5/2} \rightarrow 6p_{1/2}; 7p_{1/2}$, $5f_{7/2} \rightarrow 6p_{3/2}; 7p_{3/2}$, $5g_{7/2} \rightarrow 5g_{9/2}$, $6p_{1/2} \rightarrow 6p_{3/2}$ and $7p_{1/2} \rightarrow 7p_{3/2}$. High impact of correlations are observed for $5d_{3/2} \rightarrow 7s_{1/2}; 8s_{1/2}$, $5d_{5/2} \rightarrow 7s_{1/2}; 8s_{1/2}$ transitions. These transitions are correlated by about 12%, 30%, 18% and 28%, respectively. The correlation contributions to all the other transitions are less than 10 %. FIG. 3 shows the percentage contributions of direct and exchange core polarization parts for the $E2$ transitions. In all the strong contributing cases, the direct and exchange parts are opposite in sign. In spite of the strong contributions from direct and exchange terms, the total core polarization contributions turn out to be small due to cancellation among the terms for most of the cases. Only for $5f_{5/2} \rightarrow 6p_{3/2}$ and $5f_{7/2} \rightarrow 6p_{3/2}$ transitions, both the parts give negative contributions.

The $M1$ transition amplitudes are presented in Table IV along with the different correlation contributions and transition wavelengths. As expected our results are consistent with

earlier calculations [43, 54, 55, 70, 71] on these magnetic dipole transitions for other atomic ion species. Transition amplitude of $5d_{3/2} \rightarrow 5d_{5/2}$ for W VI available in literature using the HFR+CPOL method [41], agreeing with the present result within 0.2%. The strong amplitudes between the fine structure states of same ^{2S+1}L level are dominated by the DF values and have correlation contributions less than 0.1%. Therefore, the DF calculations for the $M1$ transitions between the fine structure states are excellent approximations. Unlike $E1$ and $E2$ transition, in these cases, core correlation contributions are significant.

The life times of the first and second excited states are presented in Table V. Both the lifetimes are calculated using the RCC forbidden transitions ($E2$ and $M1$) amplitudes and corresponding experimental wavelengths. Our calculations show the metastable state $5d_{5/2}$ has life time of about 0.14 second which can be verified in the EBIT experiment [11, 72] and will be good candidate for heavy ion storage ring [73]. Since the $E2$ and $M1$ matrix elements have almost same values, the lifetime of the $5d_{5/2}$ state is almost controlled by the $M1$ transition. HFR+CPOL [41] calculations of lifetime are well agreed with our results.

The hyperfine structure constants A and B of W VI with mass number 183 and nuclear spin $1/2$ are presented in Tables VI and VII, respectively. This will be one of the important contributors for high resolution spectroscopy. Both these constants are presented with different correlation contributions. The hyperfine A values have correlation contributions within 7% to 34% except for the states $5d_{5/2}$, $5f_{5/2}$, $5f_{7/2}$ and $5g_{9/2}$ where contributions are 55%, 79%, 144% and 181%, respectively. Here most of the cases, the core polarization and pair correlation contributions are comparable except in the cases of $5d_{5/2}$, $5f_{7/2}$ and $5g_{9/2}$ states, where contributions for the former correlation are one order more than latter. For $6s_{1/2}$ and $6p_{1/2}$, the pair correlation contributions are the largest. As seen from the Table VII, the B constants of $5f_{5/2}$, $5f_{7/2}$, $5g_{7/2}$ and $5g_{9/2}$ are correlated abnormally. Similar kind of features are observed in many other systems, like, In III [54], Ga III [55], Sc III [59] where core polarization is much larger than DF values. For other states, B constants are correlated by about 22% to 28%. Using these two hyperfine parameters, the hyperfine energy splitting can be calculated easily using Eq. (4). Fig. 4 and Fig. 5, depict the strengths of direct and exchange parts of the core polarization for A and B constants, respectively. For A -values, the exchange part of core polarization contributes are significantly large over its direct contributions. Whereas, the direct part of core polarization contributes appreciably compare to the exchange part for B -values except for $6p_{3/2}$ and $7p_{3/2}$ states. For the lower energy

states presented in the figure, the above two parts are of opposite signs; therefore, the strong contribution of direct parts for these states are diminished by their exchange parts.

In Table [VIII](#) and [IX](#), we have shown the hyperfine structure constants for the different stable isotopes of W VI. We consider the isotopes having mass number 182, 183, 184, 186 with corresponding nuclear spin values 2, 0.5, 4, 2. Results in these tables are important for line-profile measurements of absorption and emission lines of W VI in different astronomical bodies, and hence to get accurate picture of abundances of tungsten.

IV. CONCLUSION

We have calculated the transition amplitudes of allowed ($E1$) and forbidden ($E2$ and $M1$) transitions for W VI using a highly correlated relativistic coupled-cluster theory. Hyperfine structure A and B constants of the various low-lying states and isotopes of this element are estimated where comparison could not be done due to lack of theoretical or experimental endeavour. Importance of consideration of pair correlation in the many-body approaches are studied along with detail of core polarization correlation contributions. Good agreements are achieved between the electric dipole matrix elements based on length gauge and velocity gauges which somewhat determines the accuracy calculations. Our correlation exhaustive many-body approach provide scope to experimentalists to test their up to date technologies. The forbidden infra-red and optical transitions among the fine structure levels of the $5d$ and $6p$ terms, respectively, are very important for laser spectroscopy, plasma research and different atomic physics experiments. Our spectroscopic estimations of these allowed and forbidden transition lines mitigate the demand of high resolution data observed from stellar and interstellar medium. Our hyperfine data for various isotopes are also supplement to this.

ACKNOWLEDGMENTS

The calculations carried out in the IBM cluster at IIT-Kharagpur, India funded by DST-INSPIRE.

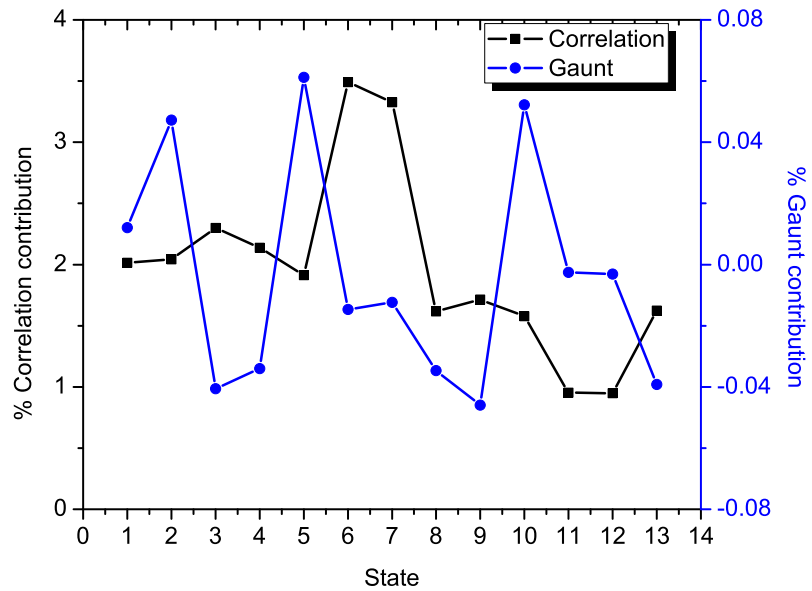


FIG. 1. Percentage of correlation and Gaunt contributions to the energy levels. Here numbers in the horizontal axis refer to the different energy states. They are 1→ $5d_{3/2}$, 2→ $5d_{5/2}$, 3→ $6s_{1/2}$, 4→ $6p_{1/2}$, 5→ $6p_{3/2}$, 6→ $5f_{5/2}$, 7→ $5f_{7/2}$, 8→ $7s_{1/2}$, 9→ $7p_{1/2}$, 10→ $7p_{3/2}$, 11→ $5g_{7/2}$, 12→ $5g_{9/2}$, 13→ $8s_{1/2}$.

TABLE I. Calculated $E1$ transition amplitudes in length gauge with the correlation contributions (in a.u.) and velocity gauge results are kept for comparison. The experimental wavelengths λ from the NIST are presented in Å. For some transitions, RCC wavelengths are used and are marked by *.

Transition	λ	Length gauge				Velocity gauge		
		DF	Core corr	Pair corr	Core pol	RCC	DF	RCC
$5d_{3/2} \rightarrow 5f_{5/2}$	382.14	2.2130	-0.0086	0.0119	-0.5229	1.6776	2.0858	1.6587
	$\rightarrow 6p_{1/2}$	677.72	-1.3542	-0.0004	0.0326	0.1327	-1.1920	-1.1568 -1.0287
	$\rightarrow 6p_{3/2}$	605.92	0.5427	0.0007	-0.0153	-0.0410	0.4886	0.4651 0.4224
	$\rightarrow 7p_{1/2}$	325.84*	0.3037	0.0000	-0.0225	-0.0913	0.1983	0.2469 0.1622
	$\rightarrow 7p_{3/2}$	317.09*	0.1408	0.0002	-0.0083	-0.0284	0.1076	0.1160 0.0878
$5d_{5/2} \rightarrow 5f_{5/2}$	395.30	-0.6120	0.0025	-0.0082	0.1355	-0.4770	-0.5739	-0.4601
	$\rightarrow 5f_{7/2}$	394.13	2.7283	-0.0113	0.0325	-0.5826	2.1467	2.5639 2.0760
	$\rightarrow 6p_{3/2}$	639.68	1.7196	0.0013	-0.0240	-0.1212	1.5776	1.4549 1.3516
	$\rightarrow 7p_{3/2}$	325.27*	0.4291	0.0002	-0.0302	-0.0825	0.3251	0.3462 0.2627
	$5f_{5/2} \rightarrow 5g_{7/2}$	994.62	5.3059	-0.0008	-0.2423	-0.2684	4.7550	5.2420 4.4892
$5f_{7/2} \rightarrow 5g_{7/2}$	1002.08	-1.0240	0.0002	0.0440	0.0514	-0.9218	-1.0109	-0.8595
	$\rightarrow 5g_{9/2}$	1001.96	6.0599	-0.0010	-0.2604	-0.3042	5.4548	5.9848 5.0864
$6s_{1/2} \rightarrow 6p_{1/2}$	1467.95	-1.9924	-0.0003	0.0386	0.2323	-1.7210	-1.8953	-1.6888
	$\rightarrow 6p_{3/2}$	1168.14	-2.7964	-0.0005	0.0560	0.3090	-2.4312	-2.6409 -2.3606
	$\rightarrow 7p_{1/2}$	434.60*	-0.1084	0.0001	-0.0142	-0.1092	-0.2182	-0.1215 -0.1968
	$\rightarrow 7p_{3/2}$	419.18*	-0.0590	-0.0001	0.0169	0.1624	0.1032	-0.0216 0.0941
	$7s_{1/2} \rightarrow 6p_{1/2}$	761.26	-1.0112	0.0001	0.0112	-0.0379	-1.0241	-0.9791 -0.9742
$7s_{1/2} \rightarrow 6p_{3/2}$	878.13	-1.7878	0.0002	0.0112	-0.0287	-1.7860	-1.7070	-1.6924
	$\rightarrow 7p_{1/2}$	3436.07*	-3.4689	0.0000	0.0564	0.1118	-3.2932	-3.4229 -3.2906
	$\rightarrow 7p_{3/2}$	2662.05*	4.8206	0.0001	-0.0823	-0.1430	4.5853	4.6091 4.4304
	$8s_{1/2} \rightarrow 6p_{1/2}$	452.57*	0.3542	-0.0001	-0.0045	0.0245	0.3711	0.3403 0.3255
$8s_{1/2} \rightarrow 6p_{3/2}$	492.08*	0.5639	-0.0002	-0.0077	0.0160	0.5692	0.5283	0.5053
	$\rightarrow 7p_{1/2}$	1656.56*	-1.8843	0.0000	0.0385	-0.0387	-1.8651	-1.8813 -1.7889
	$\rightarrow 7p_{3/2}$	1926.63*	3.3418	0.0000	-0.0524	0.0380	3.3003	3.2215 3.1125

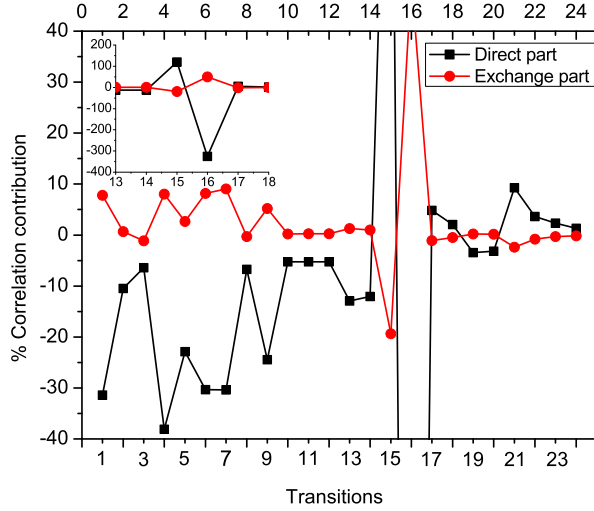


FIG. 2. Percentage of the direct and exchange parts of core polarization contributions to the $E1$ transitions. Here numbers in the horizontal axis refer to the following electronic transitions: 1=5d_{3/2} \rightarrow 5f_{5/2}, 2=5d_{3/2} \rightarrow 6p_{1/2}, 3=5d_{3/2} \rightarrow 6p_{3/2}, 4=5d_{3/2} \rightarrow 7p_{1/2}, 5=5d_{3/2} \rightarrow 7p_{3/2}, 6=5d_{5/2} \rightarrow 5f_{5/2}, 7=5d_{5/2} \rightarrow 5f_{7/2}, 8=5d_{5/2} \rightarrow 6p_{3/2}, 9=5d_{5/2} \rightarrow 7p_{3/2}, 10=5f_{5/2} \rightarrow 5g_{7/2}, 11=5f_{7/2} \rightarrow 5g_{7/2}, 12=5f_{7/2} \rightarrow 5g_{9/2}, 13=6s_{1/2} \rightarrow 6p_{1/2}, 14=6s_{1/2} \rightarrow 6p_{3/2}, 15=6s_{1/2} \rightarrow 7p_{1/2}, 16=6s_{1/2} \rightarrow 7p_{3/2}, 17=7s_{1/2} \rightarrow 6p_{1/2}, 18=7s_{1/2} \rightarrow 6p_{3/2}, 19=7s_{1/2} \rightarrow 7p_{1/2}, 20=7s_{1/2} \rightarrow 7p_{3/2}, 21=8s_{1/2} \rightarrow 6p_{1/2}, 22=8s_{1/2} \rightarrow 6p_{3/2}, 23=8s_{1/2} \rightarrow 7p_{1/2}, 24=8s_{1/2} \rightarrow 7p_{3/2}. Inset of this figure shows the same plot but in different range of horizontal and vertical axis.

TABLE II. Weighted oscillator strengths of $E1$ transitions in length (gf_L) and velocity (gf_V) gauges (in a.u.) along with the experimental wavelengths (in Å) and their comparisons with the other results (Others) .

Transition	λ	gf_L	gf_V	Others
$5d_{3/2} \rightarrow 5f_{5/2}$	382.14	2.237	2.187	$2.008^a, 1.9055^b, 1.800^c$
$\rightarrow 6p_{1/2}$	677.72	0.637	0.474	$0.631^a, 0.6166^b, 0.588^c$
$\rightarrow 6p_{3/2}$	605.92	0.120	0.089	$0.119^a, 0.1380^b, 0.116^c$
$\rightarrow 7p_{1/2}$	325.84*	0.037	0.025	0.041^c
$\rightarrow 7p_{3/2}$	317.09*	0.011	0.007	0.013^c
$5d_{5/2} \rightarrow 5f_{5/2}$	395.30	0.175	0.163	$0.154^a, 0.1318^b, 0.138^c$
$\rightarrow 5f_{7/2}$	394.13	3.552	3.321	$3.195^a, 2.6303^b, 2.820^c$
$\rightarrow 6p_{3/2}$	639.68	1.182	0.867	$1.145^a, 1.1749^b, 1.092^c$
$\rightarrow 7p_{3/2}$	325.27*	0.099	0.064	0.116^c
$5f_{5/2} \rightarrow 5g_{7/2}$	994.62	6.905	6.155	$6.439^a, 7.0795^b$
$5f_{7/2} \rightarrow 5g_{7/2}$	1002.08	0.258	0.224	$0.241^a, 0.2630^b$
$\rightarrow 5g_{9/2}$	1001.96	9.021	7.843	$8.446^a, 9.1201^b$
$6s_{1/2} \rightarrow 6p_{1/2}$	1467.95	0.613	0.590	$0.606^a, 0.5888^b, 0.462^c$
$\rightarrow 6p_{3/2}$	1168.14	1.537	1.449	$1.521^a, 1.5136^b, 1.206^c$
$\rightarrow 7p_{1/2}$	434.60*	0.033	0.027	0.050^c
$\rightarrow 7p_{3/2}$	419.18*	0.008	0.006	0.012^c
$7s_{1/2} \rightarrow 6p_{1/2}$	761.26	0.418	0.379	$0.398^a, 0.5370^b, 0.420^c$
$\rightarrow 6p_{3/2}$	878.13	1.103	0.991	$1.045^a, 0.9332^b, 0.528^c$

$a \rightarrow$ Ref. [28], $b \rightarrow$ Ref. [41], $c \rightarrow$ Ref. [42]

TABLE III. Calculated $E2$ transition amplitudes with the different correlation contributing terms (in a.u.). The experimental wavelengths λ from the NIST are presented in Å. For some transitions, RCC wavelengths are used and are marked by *. The ‘Other^a’ indicates the results obtained from another method.

Transition	λ	DF	Core corr	Pair corr	Core pol	δ_{corr}	RCC	Other ^a
$5d_{3/2} \rightarrow 5d_{5/2}$	11482.37	-1.7155	0.0103	0.0366	0.0807	0.1231	-1.5924	-1.6610
$\rightarrow 5g_{7/2}$	276.07	3.0304	-0.0032	-0.0700	-0.0345	-0.1078	2.9226	
$\rightarrow 6s_{1/2}$	1258.95	2.9061	-0.0010	-0.0966	-0.0525	-0.1451	2.7610	2.8519
$\rightarrow 7s_{1/2}$	358.53	0.2351	0.0002	0.0143	0.0300	0.0272	0.2623	
$\rightarrow 8s_{1/2}$	272.28*	-0.1015	-0.0001	-0.0131	-0.0265	-0.0308	-0.1323	
$5d_{5/2} \rightarrow 5g_{7/2}$	282.88	-1.0713	0.0013	0.0036	0.0082	0.0133	-1.0580	
$\rightarrow 5g_{9/2}$	282.87	3.7912	-0.0045	-0.0136	-0.0323	-0.0517	3.7395	
$\rightarrow 6s_{1/2}$	1413.99	3.7129	-0.0029	-0.0842	-0.0544	-0.1390	3.5739	3.4949
$\rightarrow 7s_{1/2}$	370.09	0.3692	0.0008	0.0549	0.0314	0.0672	0.4364	
$\rightarrow 8s_{1/2}$	278.29*	-0.1585	-0.0005	-0.0274	-0.0280	-0.0447	-0.2033	
$5f_{5/2} \rightarrow 5f_{7/2}$	133511.35	-4.5606	0.0020	0.3269	0.0473	0.4121	-4.1484	
$\rightarrow 6p_{1/2}$	876.21	9.0523	0.0008	-0.4743	-0.1071	-0.6326	8.4197	
$\rightarrow 6p_{3/2}$	1034.73	-5.1391	-0.0010	0.2759	0.0558	0.3627	-4.7765	
$\rightarrow 7p_{1/2}$	2169.71*	8.8125	-0.0004	-0.7028	0.0301	-0.8323	7.9802	
$\rightarrow 7p_{3/2}$	1833.14*	4.3391	-0.0004	-0.3692	0.0183	-0.4315	3.9077	
$5f_{7/2} \rightarrow 6p_{3/2}$	1026.77	-12.6148	-0.0022	0.6548	0.1347	0.8544	-11.7603	
$\rightarrow 7p_{3/2}$	1855.56*	10.6906	-0.0009	-0.8479	0.0433	-0.9884	9.7023	
$5g_{7/2} \rightarrow 5g_{9/2}$	8333333.33	-9.5003	0.0000	0.2725	0.0162	0.2981	-9.2022	
$6p_{1/2} \rightarrow 6p_{3/2}$	5719.51	7.3339	0.0018	-0.2834	-0.1021	-0.3899	6.9439	
$\rightarrow 7p_{3/2}$	591.52*	-3.0526	0.0009	0.0444	-0.0437	0.0599	-2.9927	
$6p_{3/2} \rightarrow 7p_{1/2}$	700.02*	-4.8266	0.0008	0.0525	-0.0354	0.0805	-4.7461	
$\rightarrow 7p_{3/2}$	660.88*	4.0170	-0.0009	-0.0381	0.0411	-0.0561	3.9608	
$7p_{1/2} \rightarrow 7p_{3/2}$	11817.53*	-22.7635	-0.0004	0.9392	0.0434	1.0574	-21.7061	

^a → Ref. [41]

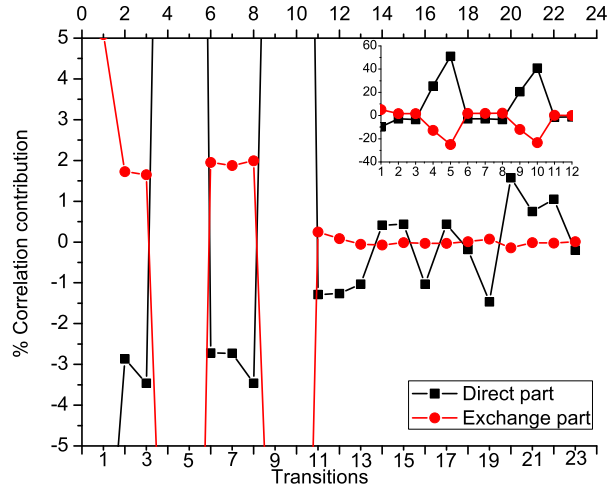


FIG. 3. Percentage of the direct and exchange parts of core polarization contributions to the $E2$ transitions. Here numbers in the horizontal axis refer to the following electronic transitions: 1= $5d_{3/2} \rightarrow 5d_{5/2}$, 2= $5d_{3/2} \rightarrow 5g_{7/2}$, 3= $5d_{3/2} \rightarrow 6s_{1/2}$, 4= $5d_{3/2} \rightarrow 7s_{1/2}$, 5= $5d_{3/2} \rightarrow 8s_{1/2}$, 6= $5d_{5/2} \rightarrow 5g_{7/2}$, 7= $5d_{5/2} \rightarrow 5g_{9/2}$, 8= $5d_{5/2} \rightarrow 6s_{1/2}$, 9= $5d_{5/2} \rightarrow 7s_{1/2}$, 10= $5d_{5/2} \rightarrow 8s_{1/2}$, 11= $5f_{5/2} \rightarrow 5f_{7/2}$, 12= $5f_{5/2} \rightarrow 6p_{1/2}$, 13= $5f_{5/2} \rightarrow 6p_{3/2}$, 14= $5f_{5/2} \rightarrow 7p_{1/2}$, 15= $5f_{5/2} \rightarrow 7p_{3/2}$, 16= $5f_{7/2} \rightarrow 6p_{3/2}$, 17= $5f_{7/2} \rightarrow 7p_{3/2}$, 18= $5g_{7/2} \rightarrow 5g_{9/2}$, 19= $6p_{1/2} \rightarrow 6p_{3/2}$, 20= $6p_{1/2} \rightarrow 7p_{3/2}$, 21= $6p_{3/2} \rightarrow 7p_{1/2}$, 22= $6p_{3/2} \rightarrow 7p_{3/2}$, 23= $7p_{1/2} \rightarrow 7p_{3/2}$. Inset of this figure shows the same plot but in different range of horizontal and vertical axis.

TABLE IV. Calculated $M1$ transition amplitudes with the different correlation contributing terms (in a.u.). The experimental wavelengths λ from the NIST are presented in Å. For some transitions, RCC wavelengths are used and are marked by *. The 'Other^a' indicates the result obtained using another method.

Transition	λ	DF	Core corr	Pair corr	Core pol	δ_{corr}	Total	Other ^a
$5d_{3/2} \rightarrow 5d_{5/2}$	11482.37	-1.54784	0.00789	0.00040	-0.00140	-0.00139	-1.54924	-1.55288
$5f_{5/2} \rightarrow 5f_{7/2}$	133511.35	-1.85149	0.00064	0.00015	-0.00030	0.00097	-1.85051	
$5g_{7/2} \rightarrow 5g_{9/2}$	8333333.33	-2.10814	0.00001	0.00000	-0.00003	-0.00008	-2.10822	
$6p_{1/2} \rightarrow 6p_{3/2}$	5719.51	1.14487	-0.00047	-0.00056	-0.00009	-0.00061	1.14426	
$\rightarrow 7p_{3/2}$	591.52*	0.08089	-0.00032	-0.00296	0.00021	0.00389	0.08477	
$6p_{3/2} \rightarrow 7p_{1/2}$	700.02*	-0.09400	-0.00026	-0.00893	-0.00036	-0.00233	-0.09633	
$7p_{1/2} \rightarrow 7p_{3/2}$	11817.53*	-1.14243	0.00018	0.00022	0.00004	0.00035	-1.14208	

^a → Ref. [41]

TABLE V. The lifetime (in s) of $5d_{5/2}$ and $6s_{1/2}$ states. The 'Other^a' indicates the results obtained by other author.

State	Our	Other ^a
$5d_{5/2}$	1.40×10^{-1}	1.40×10^{-1}
$6s_{1/2}$	3.82×10^{-4}	3.77×10^{-4}

^a → Ref. [41]

TABLE VI. Hyperfine A constants with different correlation contributing terms (in MHz).

State	DF	Core corr	Pair corr	Core pol	δ_{corr}	RCC
$5d_{3/2}$	379.50	2.10	20.33	34.76	62.06	441.56
$5d_{5/2}$	147.14	1.30	5.66	-96.28	-80.26	66.88
$5f_{5/2}$	16.86	1.01	3.50	5.62	13.38	30.24
$5f_{7/2}$	9.42	0.47	1.83	-15.57	-13.60	-4.18
$5g_{7/2}$	0.58	0.00	0.04	0.06	-0.05	0.53
$5g_{9/2}$	0.37	0.00	0.02	-0.70	-0.67	-0.30
$6s_{1/2}$	9759.05	-158.12	920.29	860.81	1564.44	11323.50
$6p_{1/2}$	2343.47	-29.92	265.56	222.03	454.95	2798.42
$6p_{3/2}$	258.34	-1.59	28.51	53.67	87.77	346.11
$7s_{1/2}$	4243.79	-54.02	220.91	336.70	498.22	4742.01
$7p_{1/2}$	1131.38	-10.82	79.28	94.87	165.08	1296.46
$7p_{3/2}$	129.14	-0.44	10.38	23.73	41.62	170.76
$8s_{1/2}$	2931.87	-33.73	18.11	222.04	203.73	3135.59

 TABLE VII. Hyperfine B constants with different correlation contributing terms (in MHz).

State	DF	Core corr	Pair corr	Core pol	δ_{corr}	RCC
$5d_{3/2}$	-1958.31	-38.74	-105.78	-287.29	-427.60	-2385.91
$5d_{5/2}$	-2321.05	-50.07	-89.60	-477.65	-607.46	-2928.52
$5f_{5/2}$	-131.78	-7.80	-27.37	-372.74	-349.28	-481.06
$5f_{7/2}$	-153.22	-8.86	-29.93	-445.18	-419.46	-572.68
$5g_{7/2}$	-5.66	-0.08	-0.38	-213.43	-206.36	-212.02
$5g_{9/2}$	-6.19	-0.09	-0.41	-233.46	-225.87	-232.06
$6p_{3/2}$	-3946.23	44.64	-434.43	-736.07	-1113.48	-5059.71
$7p_{3/2}$	-1972.79	14.65	-158.56	-315.91	-464.47	-2437.25

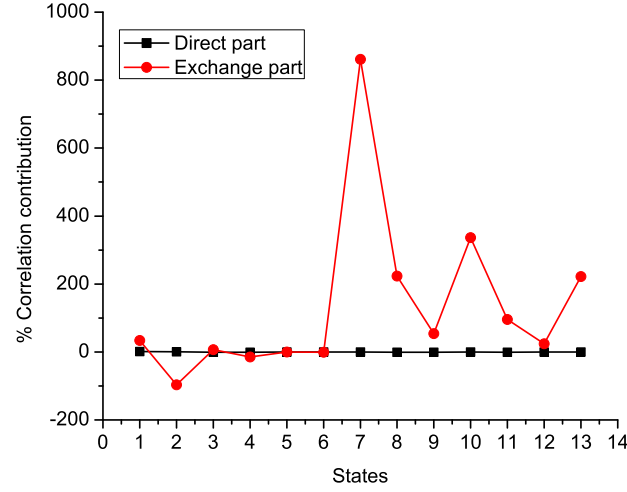


FIG. 4. Percentage of the direct and exchange parts of core polarization contributions to the hyperfine A constants. Here numbers in the horizontal axis refer to the following states: 1=5d_{3/2}, 2=5d_{5/2}, 3=5f_{5/2}, 4=5f_{5/2}, 5=5g_{7/2}, 6=5g_{9/2}, 7=6s_{1/2}, 8=6p_{1/2}, 9=6p_{3/2}, 10=7s_{1/2}, 11=7p_{1/2}, 12=7p_{3/2}.

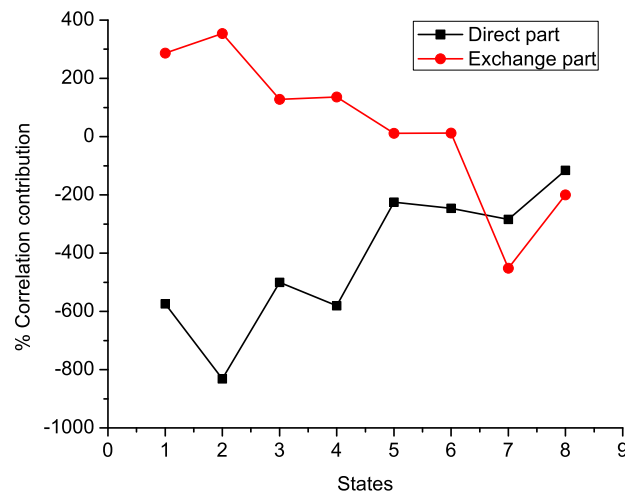


FIG. 5. Percentage of the direct and exchange parts of core polarization contributions to the hyperfine B constants. Here numbers in the horizontal axis refer to the following states: 1=5d_{3/2}, 2=5d_{5/2}, 3=5f_{5/2}, 4=5f_{5/2}, 5=5g_{7/2}, 6=5g_{9/2}, 7=6p_{3/2}, 8=7p_{3/2}.

TABLE VIII. Hyperfine A constants (in MHz) for different isotopes of W VI. The parenthesis indicate mass numbers of the isotopes.

State	$A(182)$	$A(183)$	$A(184)$	$A(186)$
$5d_{3/2}$	488.30	441.56	541.70	576.36
$5d_{5/2}$	73.94	66.88	82.05	87.33
$5f_{5/2}$	33.44	30.24	37.09	39.46
$5f_{7/2}$	-4.62	-4.18	-5.12	-5.44
$5g_{7/2}$	0.59	0.53	0.65	0.70
$5g_{9/2}$	-0.33	-0.30	-0.37	-0.39
$6s_{1/2}$	12522.97	11323.50	13890.60	14777.21
$6p_{1/2}$	3094.63	2798.42	3433.08	3652.71
$6p_{3/2}$	382.74	346.11	424.61	451.78
$7s_{1/2}$	5244.32	4742.01	5817.06	6188.35
$7p_{1/2}$	1433.69	1296.46	1590.49	1692.24
$7p_{3/2}$	188.83	170.76	209.48	222.89
$8s_{1/2}$	3467.74	3135.59	3846.46	4091.98

TABLE IX. Hyperfine B constants (in MHz) for different isotopes of W VI. The parenthesis indicate mass numbers of the isotopes.

State	$B(182)$	$B(183)$	$B(184)$	$B(186)$
$5d_{3/2}$	-2871.18	-2385.91	-2520.71	-2116.31
$5d_{5/2}$	-3524.15	-2928.52	-3093.96	-2597.60
$5f_{5/2}$	-578.90	-481.06	-508.23	-426.70
$5f_{7/2}$	-689.17	-572.68	-605.04	-507.97
$5g_{7/2}$	-255.15	-212.02	-224.00	-188.06
$5g_{9/2}$	-279.26	-232.06	-245.17	-205.84
$6p_{3/2}$	-6088.80	-5059.71	-5345.56	-4487.99
$7p_{3/2}$	-2932.97	-2437.25	-2574.95	-2161.86

[1] J. Clementson, T. Lennartsson, and P. Beiersdorfer, Atoms, **3**, 407 (2015).

[2] M. Reinke, P. Beiersdorfer, N. T. Howard, E. W. Magee, Y. Podpaly, J. E. Rice, and J. L. Terry Rev. Sci. Instrum. **81**, 10D736, (2010).

[3] V. Riccardo, M. Firdaouss, E. Joffrin, G. Matthews, P. Mertens, V. Thompson, and E. Villedieu, Phys. Scr. T, **138**, 014033 (2009).

[4] V. Rohde, M. Balden, T. Lunt, and the ASDEX Upgrade Team, Phys. Scr. **2009**, 014024 (2009).

[5] R. R. Rakhimov, D. E. Jones, H. L. Rocha, A. I. Prokof'ev, and A. I. Aleksandrov, J. Phys. Chem. B, **104**, 10973 (2000).

[6] Y. Mei, C. -F Wei, W. -C Zheng, Physica B: Condensed Matter Volume **483**, 78 (2016).

[7] D. E. J. Armstrong, X. Yi, E. A. Marquis, and S. G. Roberts, Journal of Nuclear Materials **432**, 428 (2013).

[8] A. Miyahara and R. Behrisch, Journal of Nuclear Materials, **179**, 1231 (1991).

[9] R. Behrisch, Atomic and Plasma-Material Interaction Data for Fusion, **1**, 7 (1991).

[10] M.S. Safronova, V.A. Dzuba, V.V. Flambaum, U.I. Safronova, S.G. Porsev, and M.G. Kozlov, Phys. Rev. Lett. **113**, 030801 (2014).

[11] A Müller, Atoms, **3**, 120 (2015).

[12] M. J. Seaton, Mon. Not. R. Astron. Soc. **114**, 154 (1954).

[13] M. J. Seaton and D. E. Osterbrock, Astrophys. J. **125**, 66 (1957).

[14] E. Biemont and C. J. Zeippen, Comment. At. Mol. Phys. **33**, 29 (1996).

[15] D. -C. Lee, A. N. Halliday, I. Leya, R. Wieler, U. Wiechert, Earth and Planetary Science Letters **198**, 267 (2002).

[16] J. Masarik, Earth and Planetary Science Letters **152**, 181 (1997).

[17] S. Casassus, P. J. Storey, M. J. Barlow and P. F. Roche, MNRAS, **359**, 1386 (2005).

[18] Y. Podpaly, J. Clementson, P. Beiersdorfer, J. Williamson, G. V. Brown, and M. F. Gu, Phys. Rev. A **80**(5), 052504 (2009).

[19] J. Clementson, P. Beiersdorfer, and M. F. Gu Phys. Rev. A **81**(1), 012505 (2010).

[20] A. E. Kramida and J. Reader, At. Data Nucl. Data Tables **92**, 457 (2006).

[21] A. E. Kramida and T. Shirai, At. Data Nucl. Data Tables **95**, 305 (2009).

- [22] S. D. Loch, M. S. Pindzola, C. P. Ballance, D. C. Griffin, A. D. Whiteford, and T. Pütterich, AIP Proc. **874**, 233 (2006).
- [23] U. I. Safronova, A. S. Safronova, and P. Beiersdorfer, J. Phys. B **45**, 085001 (2012).
- [24] U. I. Safronova, A. S. Safronova, P. Beiersdorfer, and W. R. Johnson, J. Phys. B: At. Mol. Opt. Phys. **44**, 035005 (2011).
- [25] U. I. Safronova, A. S. Safronova, and P. Beiersdorfer, J. Phys. B: At. Mol. Opt. Phys. **42**, 165010 (2009).
- [26] F. G. Meijer, Physica **73**, 415 (1974).
- [27] J. Sugar and V. Kaufman, Phys. Rev. A **12**, 994 (1975).
- [28] U. I. Safronova and A. S. Safronova, Phys. Rev. A **85**, 032507 (2012).
- [29] C. Biedermann, R. Radtke, R. Seidel, and E. Behar, J. Phys. Conf. Series **163**, 012034 (2009).
- [30] J. Clementson, P. Beiersdorfer, M. F. Gu, H. S. McLean, and R. D. Wood, J. Phys. Conf. Ser. **130**, 001204 (2008).
- [31] C. Biedermann, R. Radtke, R. Seidel, and T. Pütterich, Phys. Scr. T **134**, 014026 (2009).
- [32] F.-C. Meng, L. Zhou, M. Huang, C.-Y. Chen, Y.-S. Wang, and Y.-M. Zou, J. Phys. B: At. Mol. Opt. Phys. **42**, 105203 (2009).
- [33] C. Biedermann and R. Radtke, AIP Conf. Proc. **1161**, 95 (2009).
- [34] F.-C. Meng, C.-Y. Chen, Y.-S. Wang, and Y.-M. Zou, J. Quant. Spectrosc. Radiat. Transf. **109**, 2000 (2008).
- [35] S. Schippers, D. Bernhardt, A. Müller, C. Krantz, M. Grieser, R. Repnow, A. Wolf, M. Lestinsky, M. Hahn *et al.* Phys. Rev. A **83**, 012711 (2011).
- [36] E. Behar, P. Mandelbaum, and J. L. Schwob, Phys. Rev. A **59**, 2787 (1999).
- [37] S. Dalhed, J. Nilsen, and P. Hagelstein, Phys. Rev. A **33**, 264 (1986).
- [38] E. Behar, A. Peleg, R. Doron, P. Mandelbaum, and J. L. Schwob, J. Quant. Spectrosc. Radiat. Transf. **58**, 449 (1997).
- [39] C. P. Ballance, S. D. Loch, M. S. Pindzola, and D. C. Griffin, J. Phys. B: At. Mol. Opt. Phys. **43**, 205201 (2010).
- [40] E. Behar, R. Doron, P. Mandelbaum, and J. L. Schwob, Phys. Rev. A **61**, 062708 (2000).
- [41] S. E. Yoca, P. Palmeri, P. Quinet, G. Jumet and É. Biémont, J. Phys. B: At. Mol. Opt. Phys. **45**, 035002 (2012).
- [42] J. Migdalek and W. Siegel, J. Phys. B: At. Mol. Opt. Phys. **47**, 075003 (2014).

[43] G. Dixit, B. K. Sahoo, R. K. Chaudhuri, and S. Majumder, Phys. Rev. A **76**, 042505 (2007).

[44] G. Dixit, H. S. Nataraj, B. K. Sahoo, R. K. Chaudhuri, and S. Majumder, Phys. Rev. A **77**, 012718 (2008).

[45] N. N. Dutta and S. Majumder, Indian J. Phys., **90**, 373 (2016).

[46] R. F. Bishop, and H. G. Kümmel, Physics Today March **40**, 52 (1987).

[47] E. Ilyabaev, and U. Kaldor, Chem. Phys. Lett. **194**, 95 (1992); Phys. Rev. A **47**, 137 (1993).

[48] I. Lindgren, and D. Mukherjee, Physics Reports **151**, 93 (1987).

[49] M. Urban, J. Noga, S. J. Cole, and R. J. Bartlett, J. Chem. Phys. **83**, 4041 (1985).

[50] K. Raghavachari, G. W. Trucks, J. A. Pople, and M. Head-Gordon, Chem. Phys. Lett. **157**, 479 (1989).

[51] R. K. Chaudhuri, B. K. Sahoo, B. P. Das, H. Merlitz, U. S. Mahapatra, J. Chem. Phys. **119**, 10633 (2003).

[52] B. K. Mani, K. V. P. Latha, and D. Angom, Phys. Rev. A **80**, 062505 (2009).

[53] B. K. Mani, and D. Angom, Phys. Rev. A **83**, 012501 (2011).

[54] S. Roy, N. N. Dutta and S. Majumder, Phys. Rev. A, **89**, 042511 (2014).

[55] N. N. Dutta, S. Roy, G. Dixit, and S. Majumder Phys. Rev. A, **87**, 012501 (2013).

[56] S. Roy and S. Majumder, Phys. Rev. A, **92**, 012508 (2015).

[57] N. N. Dutta and S. Majumder, Phys. Rev. A, **90**, 012522 (2014).

[58] N. N. Dutta, and S. Majumder, Astrophys. J., **737**, 25 (2011).

[59] N. N. Dutta, S. Roy, and P. C. Deshmukh, Phys. Rev. A **92**, 052510 (2015).

[60] I. P. Grant, J. Phys. B **7**, 1458 (1974).

[61] W. R. Johnson, D. R. Plante, and J. Sapirstein, Adv. At. Mol. Opt. Phys. **35**, 255 (1995).

[62] P. K. Mondal, N. N. Dutta, G. Dixit and S. Majumder, Phys. Rev. A, **87**, 062502 (2013).

[63] I. Lindgren and J. Morrison, *Atomic Many-body Theory*, edited by G. Ecker, P. Lambropoulos, and H. Walther (Springer, Berlin, 1985), Vol. **3**.

[64] K. T. Cheng and W. J. Childs, Phys. Rev. A **31**, 2775 (1985).

[65] E. Clementi (Ed.), *Modern Techniques in Computational Chemistry: MOTECC-90*, (ESCOM Science Publishers B. V., 1990).

[66] F. A. Parpia, C. F. Fischer, and I. P. Grant, Comput. Phys. Commun., **175**, 745 (2006).

[67] A. Kramida, Y. Ralchenko, J. Reader, and NIST ASD Team (2015). NIST Atomic Spectra Database (ver. 5.3), <http://physics.nist.gov/asd> [2015, December 27]. National Institute of

Standards and Technology, Gaithersburg, MD.

- [68] I. P. Grant, *Relativistic Quantum Theory of Atoms and Molecules: Theory and Computation*, (Springer, 2007).
- [69] G. Gopakumar, H. Merlitz, R. K. Chaudhuri, B. P. Das, U. S. Mahapatra and D. Mukherjee, Phys. Rev. A **66**, 032505 (2002).
- [70] U. I. Safronova and M. S. Safronova, Can. J. Phys. **89**, 465 (2011).
- [71] U. I. Safronova, and M. S. Safronova, Phys. Rev. A **89**, 052515 (2014).
- [72] F J. Currell, 'Electron Beam Ion Traps and their Use in the Study of Highly Charged Ions'. In 'The Physics of Multiply and Highly Charged Ions', **1**, 39, Currell, F., Ed.; Kluwer Academic Publishers: Dordrecht, The Netherlands, (2003).
- [73] S. Schippers, Nucl. Instrum. Meth. in Phys. Res. **350**, 61, (2015).